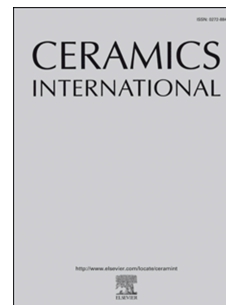# Journal Pre-proof

Calcium aluminate cement in castable alumina: From hydrate bonding to the *in situ* formation of calcium hexaluminate

Rafael Salomão, Mirian A. Kawamura, Ana B.V. Emilio, José Sakihama, Ana M. Segadães

Please cite this article as: R. Salomão, M.A. Kawamura, A.B.V. Emilio, J. Sakihama, A.M. Segadães, Calcium aluminate cement in castable alumina: From hydrate bonding to the *in situ* formation of calcium hexaluminate, *Ceramics International*, https://doi.org/10.1016/j.ceramint.2021.02.066.

This is a PDF file of an article that has undergone enhancements after acceptance, such as the addition of a cover page and metadata, and formatting for readability, but it is not yet the definitive version of record. This version will undergo additional copyediting, typesetting and review before it is published in its final form, but we are providing this version to give early visibility of the article. Please note that, during the production process, errors may be discovered which could affect the content, and all legal disclaimers that apply to the journal pertain.

Calcium aluminate cement in castable alumina: From hydrate bonding to the *in situ* formation of calcium hexaluminate

*Rafael Salomão[1], Mirian A. Kawamura[1], Ana B.V. Emilio[1], José Sakihama[2], Ana M. Segadães[3]

[1] Materials Engineering Department, São Carlos School of Engineering, University of São Paulo

Avenida Trabalhador São-carlense 400 São Carlos, Brazil

rsalomao@sc.usp.br

[2] Mechanical Enginering Department, Pontificia Universidad Católica del Perú

Avenida Universitaria 1801, Lima, Peru

jsakihama@pucp.edu.pe

[3] Department of Materials and Ceramic Engineering (CICECO), University of Aveiro, Aveiro, Portugal

segadaes@ua.pt

ABSTRACT

Calcium hexaluminate (CA_6) is an intrinsically densification-resistant material, therefore, its porous structures are key materials for applications as high-temperature thermal insulators. This article reports on the combination of calcined alumina and calcium aluminate cement (CAC) in castable aqueous suspensions for the *in situ* production of porous CA_6. The CAC content (10-34 vol.%) and the curing conditions ensure structural integrity prior to sintering and maximize the development of hydrated phases. Changes in physical properties, crystalline phases, and microstructure were investigated after isothermal treatments (120-1500°C), and three sequential porogenic events were observed. The hydration of CAC preserved the water-derived pores (up to 120°C), and the dehydroxylation of CAC hydrates (250-700°C) generated inter-particles pores. Moreover, the *in situ* expansive formation of CA_2 and CA_6 (900-1500°C) hindered densification and generated intra-particle pores. Such events differed from those observed with other CaO sources, and resulted in significantly higher pores content and lower thermal conductivity.

Key-words: Calcium hexaluminate, alumina, calcium aluminate cement, porous ceramics.

* Corresponding author. Phone: +55 16 33739576; +351 913828655; E-mail address: rsalomao@sc.usp.br (Rafael Salomão, Salomão, R.). Avenida Trabalhador São-carlense 400 13566-590 São Carlos, SP - Brazil

1. Introduction

Porous structures of calcium hexaluminate ($CaAl_{12}O_{19}$ or CA_6) show refractoriness and chemical resistance and are used as hot-air filtering elements, catalyst carriers, and high-temperature thermal insulators [1]. When compared to other ceramic materials used in the same applications, such as α-Al_2O_3 [2,3] and mullite ($Al_6Si_4O_{16}$) [4], CA_6 resists long-lasting densification, even when exposed to high temperatures for extended periods [5,6] due to two major causes. Firstly, when produced by solid-state reactions between Al_2O_3 and CaO, CA_6 results in a significant volume expansion and consequent decrease in density (final density ranges from 3.5 up to 3.7 $g.cm^{-3}$, whereas that of α-Al_2O_3 is 3.8-4.0 $g.cm^{-3}$) [7,8]. Secondly, its typically asymmetrical plate-like crystals [5,6] grow over each other, resulting in a microstructure with a large portion of intra-particle pores [9-11]. Because such pores have a high number of faces and few contact points amongst the surrounding particles, the material shows intrinsic densification resistance.

The reactions involved in solid-state CA_6 formation start at the interface between the Al_2O_3 matrix and the CaO domains (from the CaO precursors), where the concentration of Ca^{2+} ions is much higher than that in other parts of the system. Consequently, CaO-rich phases ($Ca_3Al_2O_{33}$ or C_3A, $Ca_{12}Al_{14}O_{33}$ or $C_{12}A_7$, and $CaAl_2O_4$ CA) are formed first at such contact points. As heating continues, these low melting point phases melt and help to dissolve the neighboring particles, and since such liquids are progressively enriched in alumina, the Al_2O-richer compounds ($CaAl_4O_7$ or CA_2 and CA_6) crystallize. Several studies have evaluated the effects of different raw materials [12-14] and processing techniques [15-19] on the physical properties of the resulting CA_6 porous structures [20-25]. For instance, compared to the sintering of pre-reacted particles [1,26], the *in situ* formation of CA_6 from aqueous suspensions of individual oxides or their precursors is a straightforward process of substantial energy-saving potential. The porous structures produced typically show a small average pore size and higher strength, which are features particularly attractive in the production of thermal insulators [14,27]. The process requires a careful preparation of stable low-viscosity co-dispersions of particles of Al_2O_3 and CaO sources [28,29], the definition of an adequate heating schedule for the drying, dehydroxylation, and decarbonation steps [6,14], and use of hydraulic binders prior to sintering. However, little attention has been devoted to the role of such binders in the evolution of the physical properties of porous CA_6.

Hydraulic binders, such as hydratable aluminas (HA) and calcium aluminate cement (CAC), set in the presence of water and, through several chemical reactions, restrain particles'

movement strengthening the structure after casting and curing [30,31]. Important events, namely free-water withdrawal, dehydroxylation of binders' hydrates, reorganization of the microstructure, and formation of new phases take place during the initial heating of hydraulic bonded suspensions, [32]. Strength loss and porosity increase can also occur, depending on the type of bonding between the hydrate particles and the surrounding matrix [33,34].

HA has been used as calcium-free hydraulic binders and can simultaneously act as an Al_2O_3 source (ρ-Al_2O_3 is fully converted to α-Al_2O_3 above 900 °C) [3,4] in the formation of CA_6. However, HA-bonded suspensions typically require longer and intense mixing steps due to the particles' large specific surface area, and result in low permeability set structures [35,36]. Moreover, the hydraulic bonds amongst particles break during the initial heating at temperatures between 110-350 °C with a significant loss of strength [3]. CAC, on the other hand, is the most popular hydraulic binder for refractory castable systems [30,31] and, differently from HA, is less sensitive to mixing and drying conditions [37-39]. In fact, given the abundant presence of water molecules in the resulting hydrates (such as $CaAl_2O_4 \cdot (H_2O)_{10}$ or CAH_{10}, and $Ca_3Al_2O_7 \cdot (H_2O)_6$ or C_3AH_6), significant density variations occur during the first heating, and the hydrates themselves can behave as porogenic particles [32-34].

Besides the porogenic action of the combination of CAC and water on the cured and dried material, the formation of CA_6 is readily expected from the cement hydrates upon heating in the presence of a suitable source of Al_2O_3. Because the microstructure of such porous materials formed *in situ* depends strongly on the size ratio between alumina and calcia sources, the CA_6 formed from a CAC source, whose ions are mixed at an atomic level [40], might display characteristics different from those of other Al_2O_3-CaO pairs. These issues are addressed in the present article.

2. Materials and methods

Annex A describes the raw materials characterization and the methodology employed for the production of aqueous suspensions containing calcined alumina (CAl) and 10 vol.%, 20 vol.%, and 34 vol% of calcium aluminate cement (CAC), as well as the compositions and preliminary tests conducted for determining the best curing conditions and CAC load range.

The CAl-CAC suspensions were homogenized and cast under vibration as cylinders in non-adhering polymeric molds of 38 mm length × 38 mm diameter, for thermogravimetric

tests, 70 mm length $\times$ 16 mm diameter, for flexural Young's modulus, flexural strength, linear dimensional change, and total porosity measurements, and 8 mm length $\times$ 6 mm diameter, for dilatometric analysis and thermal conductivity measurements. Curing was carried out at 60 °C for 24 h periods in a moisture saturated atmosphere.

The drying and dehydroxylation behaviors of green humid freshly demolded samples (of approximately 100 g) were evaluated in tailor-made thermogravimetric equipment capable of supporting large samples (up to 500 g and up to $10 \times 10 \times 10$ cm^3) and testing both monolithic and powdered samples. It monitors and records (every 10 s) the temperature and weight changes of a sample placed in an electric furnace (further details on the technique can be found in [35]). During the thermogravimetric tests, samples were heated up to 120 °C (2 °C.min^{-1}) and kept at such temperature for 17 h for the withdrawal of non-chemically bonded water [35,36,41]). After this period, the temperature was increased (2 °C.min^{-1}) up to 800 °C for the release of combined water from hydrated compounds [35,36]. The instantaneous mass loss (W, wt%) recorded was the sample's total mass loss, and the mass loss rate (dW/dt, wt%.h^{-1}) was obtained from the former as the slope between adjacent values.

Samples for flexural Young's modulus, flexural strength, linear dimensional change, total porosity, and thermal conductivity measurements were demolded after curing and dried at 120 °C for 24 h. They were then treated at 300, 500, 700, 900, 1100, 1300, and 1500 °C (2 °C.min^{-1} heating rate; 3 h hold; 10 °C.min^{-1} cooling rate down to room temperature).

The flexural Young's modulus (E, GPa) of the heat-treated samples was measured at room temperature (25°C) and during the first heating (from 25°C up to 1500°C, 2°C.min^{-1} heating rate) by Impulse Excitation of Vibration Technique (Grindosonic HT, Belgium), according to ASTM E 1876-01 standard ("Standard Test Method for Dynamic Young's Modulus, Shear Modulus, and Poisson's Ratio by Impulse Excitation of Vibration"). The samples' flexural strength was measured at room temperature (25 °C) by three-point bending tests (MTS 810 TestStar II tensile tester; 2 N.s^{-1} loading rate; ASTM C78: "Standard Test Method for Flexural Strength of Concrete Using Simple Beam with Third-Point Loading").

The solid density was determined for dried and heat-treated samples (crushed, particles' size below 100 µm) by Helium pycnometry. In each case, the sample's geometry (diameter and length), mass, and solid density were used for the calculation of the geometrical total porosity (vol.%).

The length of hardened samples was measured after drying at 120 °C (L$_{Dried}$), and after the final heat treatment (L$_{Sintered}$). Their linear dimensional change (LDV, %) was calculated

according to the corresponding initial length (positive values represent expansion; negative ones indicate shrinkage). Each result for Young's modulus, flexural strength, total porosity, and dimensional change is the average value obtained for 5 different samples (standard deviation represented by error bars).

A continuous dilatometric analysis (DIL402C, Netzsch, Germany, 5 °C.min^{-1} heating rate up to 1500 °C) was conducted on green samples previously dried at 120 °C for 24 h.

The pore size distribution of samples sintered at 1500 °C for 3 h was assessed by mercury intrusion porosimetry (PoreMaster 33, Quantochrome Instruments, USA; 0.480 N.m^{-1} mercury surface tension, 130° contact angle, and 0.0014 and 210 MPa applied pressure). The thermal conductivity was measured from 600ºC to 1400ºC in laser flash apparatus (Netszch, LFA427, Germany) in samples sliced as cylinders of 6 mm diameter × 1 mm thickness.

The phases formed at each heat treatment temperature were identified in crushed samples (particle size below 100 µm) by X-ray diffraction (XRD, Rotaflex RV 200B, Rigaku-Denki Corp., Japan, Cu Kα radiation (λ = 0.14506 nm), in the 2θ range from 15 to 75° at 0.5 °.min^{-1} scan rate) and quantified by Rietveld method (MATCH! software, 3.8 version, Germany) [42]. The percent ratio of each phase detected is showed as a bar chart in the manuscript, whereas the full XRD patterns and compounds identification are detailed in Annex B. The microstructure was observed by field-emission-gun scanning electron microscopy (FEG-SEM, Inspect-F50, FEI, Netherlands) on fractured surfaces after gold coating.

3. Results and discussion

3.1 Particles characterization and preliminary tests

Annex A provides the results of both particles' characterization (Table 1 and Figs. A.1a-c) and tests that determined the CAC load range and the most suitable curing conditions for maximizing the hydrates formation and bonding action of the hydraulic binder (Figs. A.2 and A.3).

3.2 Evolution of samples' microstructure and physical properties upon heating up to 700 °C

Figs 1a-b show the thermogravimetric curves of freshly demolded samples, where two drying stages can be observed. From the original water content in the formulation, the fraction not consumed in the hydration reactions is called free-water, whereas the remaining one is known as chemically bonded water [35,41]. Free-water must be released at the beginning of the drying process as vapor between room temperature and 120 °C. For all compositions, a significant portion of the initial water content remained in the hardened structure as non-chemically bonded free-water. Since no significant peaks of anhydrous CAC phases were detected by XRD in dried samples (Figs. 2 and A.3) and all compositions were prepared with the same volumetric amount of water, the samples with higher CAC contents consumed a larger fraction of the original casting water during hydroxylation. As expected, the higher the initial CAC content in the formulations, the smaller the release of free water (67, 78, and 88 wt% of the corresponding total, respectively for samples containing 34, 20, and 10 vol.% of CAC) [43]. Fig. 3a and A.1d-f (Annex A) show such samples' microstructure, comprised of a mixture of α-Al_2O_3, C_3AH_6, and $Al(OH)_3$ (Fig. 2; see Fig. B.1 in Annex B for complete XRD patterns), as in [37-39,44].

Figure 1

Figure 2

Figure 3

After the removal of free-water, rising temperatures led to the decomposition of hydroxylated compounds between 200 and 500 °C [32-35]. During heating from 120 °C up to 800 °C (Fig. 1c), samples containing heavier CAC loads (20 vol% and 34 vol%) experienced a more substantial mass loss related to the dehydroxylation of hydrates (22 wt% and 33 wt%) than those prepared with 10 vol.% of CAC (12 wt.% mass loss). The loss of combined water increased particles' density and reduced their volume, causing a progressive disappearance of bridging points amongst the particles of the α-Al_2O_3 matrix, as shown in Fig. 3b-d. Heat treatments up to 500 °C resulted in an increase in total porosity and an initial loss of strength and rigidity (Figs. 4a, 5a, and 6a), accompanied by a significant linear shrinkage between 200 and 500 °C (Figs. 4b, 5b and 6b). Such results can be explained by the dehydroxylation of

Al(OH)$_3$ and C$_3$AH$_6$ (in the 250-350 °C and 320-400 °C temperature ranges, respectively, [2,3,32,33]) and formation of C$_3$A (Fig. 2).

Above 500 °C, although the total porosity grows slowly, a general recovery of strength and rigidity occurs in all cases. In samples treated at 700 °C, practically all C$_3$A was converted to C$_{12}$A$_7$ and CA$_2$, which is in agreement with other studies [12,27,32]. Fig. 3d displays such compounds as thinner particles located in the space amongst the calcined alumina particles and their surfaces. The results also indicate CaO-Al$_2$O$_3$ solid-state inter-diffusion reactions, typically slow at temperature ranges below 1300 °C, were speeded-up by shorter diffusion paths and a larger contact area amongst the particles formed, and explain the formation of such CaO-richer calcium aluminates at comparable low-temperature ranges and the incipient sintering observed.

Figure 4

Figure 5

Figure 6

3.3 Evolution of samples' microstructure and physical properties during reactive sintering (900-1500 °C)

Although in all cases the dilatometry (continuous heating) showed maximum expansion rate at approximately 1180 °C, samples treated at 900 and 1100 °C for 3 h underwent a significant permanent (post-treatment) expansion (Figs. 4b, 5b, and 6b). In both cases, because such an expansion can be associated with the formation of C$_{12}$A$_7$ and CA$_2$ (Figs. 2 and 3e), the higher the CAC content in the formulation, the greater the expansion. At 1100 °C, the microstructures are mixtures of only α-Al$_2$O$_3$ and CA$_2$, and their simultaneous noticeable increase in strength and rigidity may be related to the early stages of sintering. Moreover, the localized formation of small portions of the liquid phase (Fig. 3f) due to the reaction between calcium aluminates and impurities contained in the raw materials (particularly SiO$_2$) may have strengthened the structure [31,32,45,46]. As the heating proceeds up to 1300 °C, the onset of sintering with densification can be observed in the high-temperature Young's modulus and dilatometry curves and microstructure (Fig. 3g), accompanied by a continuous decrease in total porosity, which contributes to a significant gain in rigidity and flexural

strength for all samples. The first diffraction peaks of CA_6 were also detected at this temperature (Fig. 2).

For samples sintered at 1500 °C, all calcium aluminates previously formed were converted into CA_6, and α-Al_2O_3 remained as a residual phase in the system (Fig. 7 and Table 1) and the evidence of liquid phases observed at samples treated at 1100 °C and 1300 °C (Figs. 3f-g) is no longer detected (Fig. 3h). Such an effect occurs because, above 1300 °C, the liquid comprised of CA_2 and other residual impurities begins to dissolve the surrounding alumina particles and changes its compositions to CA_6. Due to a higher melting temperature, the liquid crystallizes, displaying an asymmetrical hexagonal plate morphology, typical of CA_6 crystals [5,6,14].

The effect of the expansive formation of CA_2 and CA_6 that tends to counteract the sintering densification of the calcined alumina matrix is particularly noticeable in samples with higher CAC contents [6,47]. While samples with 10 vol% of CAC (Fig. 4a) show a continuous decrease in total porosity due to the linear shrinkage observed, those containing 20 vol% (Fig. 5a) show a deacceleration in the reduction of total porosity, and those with 34 vol% CAC experience a significant total porosity increase and lower shrinkage (Fig. 6a). CA_6 crystals intrinsically resist densification, as reviewed elsewhere [5,6], because the formation of their highly asymmetrical hexagonal plates pushes apart calcined alumina particles and other CA_6 crystals. As a consequence of the high levels of total porosity (36-50 vol.%), compositions containing 20 and 34 vol% of CAC showed smaller gains of strength and rigidity. Nevertheless, such properties' values are similar to those reported in [1,6,13,14,19,30], which tested porous CA_6 structures of comparable porosity levels.

Figure 7

3.4 Comparison of microstructure and physical properties of porous CA6 formed from CAC and other sources of CaO

The microstructure of the CAC-based porous CA_6 samples produced differs significantly from those observed in previous studies, in particular after heat treatments between 900 and 1300 °C (Fig.8). Salomão *et al.* [6] and Costa *et al.* [14], who used spherical particles (15 µm) of precipitated β-$CaCO_3$ (or calcite) and μ-$CaCO_3$ (or vaterite) as a calcia sources, detected round pores after heat treatment at 1100-1300 °C, whose final size and shape were similar to those of the original $CaCO_3$ particles. They appeared to be internally

9

lined by a glassy phase whose composition resembled a mixture of $C_{12}A_7$, CA, and CA_2. After sintering at 1500 °C, larger spherical pores remained surrounded by smaller inter-particle ones located amongst the CA_6 crystals [14]. In the present study, the CaO-source was the fine particles of hydrates homogenously distributed amongst the matrix particles (Fig. 3a). At 900 and 1100 °C, they evolved to sub-micron domains of $C_{12}A_7$ and CA_2 crystals, preserving the inter-particle pores (Figs. 3e-f) and, at 1300 °C, such crystals covered the surface of calcined alumina particles, giving rise to a percolating coral-like porous phase (Fig. 3g). At the final stage of sintering (1500 °C), typical CA_6 crystals were formed, retaining a significant fraction of fine intra-particle and inter-particle pores (Fig. 3h).

Such a difference in the microstructure can be explained by the average size of CaO domains formed during initial heating. Coarser $CaCO_3$ particles not only leave behind nearly half of their volume as empty pores, but also represent longer diffusion paths. The liquid phase that eventually forms and drains away might even contribute to increasing the average diameter of the pores. On the other hand, because Al^{3+}, $Ca^{2+,}$ and O^{2-} ions are already mixed at an atomic level [33,34,40], the finely dispersed CaO from CAC hydrates is more reactive and hardly in excess, even if only locally. The resulting calcium aluminates and dialuminates are rapidly enriched with Al_2O_3 towards the targeted hexaluminate, producing structures of significantly smaller average pore sizes and higher total porosity levels.

Figure 8

An important consequence of such fine-pores-containing microstructure is its ability to hinder heat flow represented by the low values of thermal conductivity (0.58-0.50 W.(m.K)$^{-1}$, 600-1400 °C) (Fig. 9). *Pelissari et al.* [48] highlighted pores fractions above 50 % and in the 0.5-5 µm average size range maximize the scattering of the thermal waves (or phonons) responsible for most of the heat flow in such a temperature range. Concomitantly, the great tortuousness of thin pores prevents air convection throughout the structure. These results are in good agreement with others related to systems of similar composition and physical properties [49-51], and indicate the porous castable CA_6 structures attained can potentially be applied as high-temperature thermal insulators. Further improvements in insulation ability can be achieved by, for instance, combining this methodology with other porogenic mechanisms. Such a hypothesis is currently under investigation by the authors' research group.

Figure 9

4. Conclusions

Aqueous castable suspensions of calcined alumina (CAl) and calcium aluminate cement (CAC) can be used for the production of porous calcium hexaluminate (CA_6) through *in situ* reactions. Samples containing 10-34 vol.% of CAC showed structural integrity after curing and were safely dried according to a heating schedule that favored the release of free water below 120 °C. After sintering at 1500 °C, structures of 36-50 vol.% total porosity, 86-50 GPa Young's modulus, 49-22 MPa flexural strength, and 0.5 W.(m.K)$^{-1}$ thermal conductivity were obtained. A combination of three porogenic mechanisms is proposed towards explaining the evolution of both microstructure and physical properties. The first is the hydraulic action of CAC that preserved the pores created by the addition of water during the setting, curing, and 120 °C drying steps. The second is the dehydroxylation of CAC hydrates (250-700 °C), followed by changes in density and crystalline phases that generated inter-particle pores in the alumina matrix. Finally, the third is the expansive formation of CA_2 and CA_6 crystals (900-1500 °C) that hindered the densification of the structure and generated extra intra-particle and inter-particle pores. Such mechanisms occurred more intensely in the composition containing 34 vol.% of CAC and the larger amount of hydrates, resulting in the highest total porosity values and stoichiometric CA_6 after sintering.

Differently from studies that used $CaCO_3$ particles as a CaO source, the microstructures obtained in this study contain finer pores mainly amongst the large CA_6 crystals. Such a pore geometry was associated with the smaller average size of the CAC hydrate particles, which promoted faster conversion reactions, slightly higher total porosity levels, and lower levels of thermal conductivity.

5. Acknowledgments and declaration of competing interest

competing interests (financial or personal) affected the results reported in this paper and that they cited all funding and supporting sources.

6. References

1. A. Overhoff, A. Buhr, J. Grass, H.M. Wuthnow, New microporous materials, Ceram. Forum Int. 82 (2005) 1–5.

2. Z.-Y. Deng, T. Fukasawa, M. Ando, G.-J. Zhang, T. Ohji, Microstructure and mechanical properties of porous alumina ceramics fabricated by the decomposition of aluminum hydroxide, J. Am. Ceram. Soc. 84 (2001) 2638–2644. https://doi.org/10.1111/j.1151-2916.2001.tb01065.x

3. A.D.V. Souza, R. Salomão, Evaluation of the porogenic behavior of aluminum hydoxide particles of different size distributions in castable high-alumina structures, J. Eur. Ceram. Soc. (2016) 885-897. https://doi.org/10.1016/j.jeurceramsoc.2015.11.019

4. L.L. Souza, R. Salomão, V.L. Arantes, Development and characterization of porous moldable refractory structures of the alumina-mullite-quartz system, Ceram. Int. 43 (2017) 1362-1370. https://doi.org/10.1016/j.ceramint.2016.10.093

5. C. Domínguez, J. Chevalier, R. Torrecillas, G. Fantozzi, Microstructure development in calcium hexaluminate, J. Eur. Ceram. Soc. 21 (2001) 381–387. https://doi.org/10.1016/S0955-2219(00)00143-6

6. R. Salomão, V.L. Ferreira, L.M.M. Costa, I.R. Oliveira, Effects of the initial CaO-Al_2O_3 ratio on the microstructure development and mechanical properties of porous calcium hexaluminate, Ceram. Int. 44 (2018) 2626–2631. https://doi.org/10.1016/j.ceramint.2017.11.010

7. J.M. Tulliani, G. Pàges, G. Fantozzi, L. Montanaro, Dilatometry as a tool to study a new synthesis for calcium hexaluminate, J. Therm. Anal. Calorim. 72 (2003) 1135–1140. https://doi.org/10.1023/A:1025088230882

8. L. An, H.M. Chan, K.K. Soni, Control of calcium hexaluminate grain morphology in in-situ toughened ceramic composites, J. Mater. Sci. 31 (1996) 3223–3229. https://doi.org/10.1007/BF00354672

9. A.J. Sánchez-Herencia, R. Moreno, C. Baudín, Fracture behaviour of alumina–calcium hexaluminate composites obtained by colloidal processing, J. Eur. Ceram. Soc. 20 (2000) 2575–2583. https://doi.org/10.1016/S0955-2219(00)00123-0

10. Y. Tian, Y. Qiu, Y. Chai, P. Bai, C. Gong, The effect of sintering temperature on the structure and properties of calcium hexaluminate/anorthite ceramics, Sci. Sinter. 45 (2013) 141–147. https://doi.org/10.2298/SOS1302141T

11. S. Yi, Z. Huang, J. Huang, M. Fang, Y. Liu, S. Zhang, Novel calcium hexaluminate/spinel-alumina composites with graded microstructures and mechanical properties, Sci. Rep. 4 (2015) 4333. https://doi.org/10.1038/srep04333

12. K.J. MacKenzie, M. Schmücker, M. Smith, I.J. Poplett, T. Kemmitt, Evolution of crystalline aluminates from hybrid gel-derived precursors studied by XRD and multinuclear solid state MAS NMR, Thermochim. Acta. 363 (2000) 181–188. https://doi.org/10.1016/S0040-6031(00)00630-4

13. M.F. Wu, Y.B. Li, S.J. Li, Y.W. Li, S.B. Sang, Preparation and properties of high-purity porous calcium hexaluminate material, Key Eng. Mater. 697 (2016) 547–550. https://doi.org/10.4028/www.scientific.net/KEM.697.547

14. L.M.M. Costa, J. Sakihama, R. Salomão, Characterization of porous calcium hexaluminate ceramics produced from calcined alumina and microspheres of Vaterite (μ-CaCO₃), J. Eur. Ceram. Soc. 38 (2018) 5208–5218. https://doi.org/10.1016/j.jeurceramsoc.2018.07.034

15. D.A. Fumo, M.R. Morelli, A.M. Segadães, Combustion synthesis of calcium aluminates, Mater. Res. Bull. 31 (1996) 1243–1255. https://doi.org/10.1016/0025-5408(96)00112-2

16. D. Asmi, I. Low, S. Kennedy, R. Day, Characteristics of a layered and graded alumina/calcium-hexaluminate composite, Mater. Lett. 40 (1999) 96–102. https://doi.org/10.1016/S0167-577X(99)00055-5

17. B. Dong, B. Yuan, G. Wang, K. Chen, J. Han, H. Li, Fabrication of porous SiC/calcium hexaluminate composites, J. Eur. Ceram. Soc. 36 (2016) 3889–3893. https://doi.org/10.1016/j.jeurceramsoc.2016.05.036

18. Y. Li, R. Xiang, N. Xu, Q. Wang, S. Li, M. Wu, C. Yang, Fabrication of calcium hexaluminate-based porous ceramic with microsilica addition, Int. J. Appl. Ceram. Technol. 15 (2018) 1054–1059. https://doi.org/10.1111/ijac.12868

19. B. Dong, F. Wang, J. Yu, H. Abadikhah, S.A. Khan, M. Yang, L. Hao, X. Xu, G. Wang, S. Agathopoulos, Production of calcium hexaluminate porous planar membranes with high morphological stability and low thermal conductivity, J. Eur. Ceram. Soc. 39 (2019) 4202–4207. https://doi.org/10.1016/j.jeurceramsoc.2019.06.031

20. A.L. Gentile, W.R. Foster, Calcium hexaluminate and its stability relations in the system CaO-Al₂O₃-SiO₂, J. Am. Ceram. Soc. 46 (1963) 74–76. https://doi.org/10.1111/j.1151-2916.1963.tb11679.x

21. D. Asmi, I.M. Low, Physical and mechanical characteristics of *in-situ* alumina/calcium hexaluminate composites, J. Mater. Sci. Lett. 17 (1998) 1735–1738. https://doi.org/ 10.1023/A:1006683421321

22. L. An, H.-C. Ha, H.M. Chan, High-strength alumina/alumina: calcium-hexaluminate layer composites, J. Am. Ceram. Soc. 81 (1998) 3321–3324. https://doi.org/10.1111/j.1151-2916.1998.tb02775.x

23. C. Domínguez, J. Chevalier, R. Torrecillas, L. Gremillard, G. Fantozzi, Thermomechanical properties and fracture mechanisms of calcium hexaluminate, J. Eur. Ceram. Soc. 21 (2001) 907–917. https://doi.org/:10.1016/S0955-2219(00)00274-0

24. B.A. Vázquez, P. Pena, A.H. de Aza, M.A. Sainz, A. Caballero, Corrosion mechanism of polycrystalline corundum and calcium hexaluminate by calcium silicate slags, J. Eur. Ceram. Soc. 29 (2009) 1347–1360. https://doi.org/10.1016/j.jeurceramsoc.2008.08.031

25. P.G. De La Iglesia, O. García-Moreno, R. Torrecillas, J.L. Menéndez, Influence of different parameters on calcium hexaluminate reaction sintering by Spark Plasma, Ceram. Int. 38 (2012) 5325–5332. https://doi.org/10.1016/j.ceramint.2012.03.038

26. A. Altay, C.B. Carter, P. Rulis, W.-Y. Ching, I. Arslan, M.A. Gülgün, Characterizing CA₂ and CA₆ using ELNES, J. Solid State Chem. 183 (2010) 1776–1784. https://doi.org/10.1016/j.jssc.2010.05.028

27. L.-P. Li, Y. Yan, X.-Z. Fan, Z.-H. Hu, C.-Y. Zhao, Low-temperature synthesis of calcium–hexaluminate/magnesium–aluminum spinel composite ceramics, J. Eur. Ceram. Soc. 35 (2015) 2923–2931. https://doi.org/10.1016/j.jeurceramsoc.2015.03.041

28. R. Salomão, 2018. Porogenic Behavior of Water in High-Alumina Castable Structures, Advances in Materials Science and Engineering, 2876851.

https://doi.org/10.1155/2018/2876851

29. I.R. de Oliveira, V.M.C. Leite, M.P.V.P. Lima, R. Salomão, Production of porous ceramic material using different sources of alumina and calcia, Matéria 20 (2015) 739–746. https://doi.org/10.1590/S1517-707620150003.0078

30. W.H. Gitzen, L.D. Hart, G. Maczura, Properties of some calcium aluminate cement compositions, J. Am. Ceram. Soc. 40 (1957) 158–167. https://doi.org/10.1111/j.1151-2916.1957.tb12595.x

31. K.M. Parker, J.H. Sharp, Refractory calcium aluminate cements, Trans. J. Br. Ceram. Soc. 81 (1982) 35–42.

32. N. Schmitt, J.-F. Hernandez, V. Lamour, Y. Berthaud, P. Meunier, J. Poirier, Coupling between kinetics of dehydration, physical and mechanical behaviour for high alumina castable, Cem. Concr. Res. 30 (2000) 1597–1607. https://doi.org/10.1016/S0008-8846(00)00342-2.

33. S. Maitra, S. Bose, N. Bandyopadhyay, A. Roychoudhury, Dehydration kinetics of calcium aluminate cement hydrate under non-isothermal conditions, Ceram. Int. 31 (2005) 371–374. https://doi.org/10.1016/j.ceramint.2004.06.002

34. J.F. Zapata, M. Gomez, H.A. Colorado, Calcium aluminate cements subject to high temperature, in: T. Ohji, J. Matyas, H. Colorado, R. Kanakala (Eds.), Advances in Materials Science for Environmental and Energy Technologies VI: Ceramic Transactions, Vol. 262, The American Ceramic Society, Westerville, 2017, pp. 97-105. https://doi.org/10.1002/9781119423799.ch10

35. M.D.M. Innocentini, F.A. Cardoso, M.M. Akyioshi, V.C. Pandolfelli, Drying stages during the heating of high-alumina, Ultra-Low-Cement Refractory Castables, J. Am. Ceram. Soc. 86 (2003) 1146–1148. https://doi.org/10.1111/j.1151-2916.2003.tb03438.x

36. W.H. Gitzen, L.D. Hart, Explosive spalling of refractory castables bonded with calcium aluminate cement, Bull. Am. Ceram. Soc. 40 (1961) 503–507, 510.

37. S.M. Bushnell-Watson, J.H. Sharp, The effect of temperature upon the setting behaviour of refractory calcium aluminate cements, Cem. Concr. Res. 16 (1986) 875–884. https://doi.org/10.1016/0008-8846(86)90011-6

38. S.M. Bushnell-Watson, J.H. Sharp, Further studies of the effect of temperature upon the setting behaviour of refractory calcium aluminate cements, Cem. Concr. Res. 20 (1990) 623–635. https://doi.org/10.1016/0008-8846(90)90105-7

39. P. Garcés, E.G. Alcocel, S. Chinchón, C.G. Andreu, J. Alcaide, Effect of curing temperature in some hydration characteristics of calcium aluminate cement compared with those of portland cement, Cem. Concr. Res. 27 (1997) 1343–1355. https://doi.org/10.1016/S0008-8846(97)00136-1

40. X. Cong, R.J. Kirkpatrick, Hydration of Calcium Aluminate Cements: A Solid-State ^{27}Al NMR Study, J. Am. Ceram. Soc. 76 (1993) 409–416. https://doi.org/10.1111/j.1151-2916.1993.tb03799.x

41. G.W. Scherer, Theory of drying, J. Am. Ceram. Soc. 73 (1990) 3–14. https://doi.org/10.1111/j.1151-2916.1990.tb05082.x

42. L.B. Mccusker, R.B. Von Dreele, D.E. Cox, D. Louër, P. Scardi, Rietveld refinement guidelines, J. Appl. Crystallogr. 32 (1999) 36–50. https://doi.org/10.1107/S0021889898009856

43. T.J. Chotard, A. Smith, D. Rotureau, D. Fargeot, C. Gault, Acoustic emission characterisation of calcium aluminate cement hydration at an early stage, J. Eur. Ceram. Soc. 23 (2003) 387–398. https://doi.org/10.1016/S0955-2219(02)00152-8

44. L. Prasittisopin, I. Sereewatthanawut, Dissolution, nucleation, and crystal growth mechanism of calcium aluminate cement, J. Sustain. Cem. Mater. 8 (2019) 180–197.

https://doi.org/10.1080/21650373.2018.1558132

45. A.I. Zaitsev, A.D. Litvina, N.P. Lyakishev, B.M. Mogutnov, Thermodynamics of CaO–Al$_2$O$_3$–SiO$_2$ and CaF$_2$–CaO–Al$_2$O$_3$ –SiO$_2$ melts, J. Chem. Soc. Faraday Trans. 93 (1997) 3089–3098. https://doi.org/10.1039/a700511c

46. E.Y. Sako, M.A.L. Braulio, D.H. Milanez, P.O. Brant, V.C. Pandolfelli, Microsilica role in the CA$_6$ formation in cement-bonded spinel refractory castables, J. Mater. Process. Technol. 209 (2009) 5552–5557 https://doi.org/10.1016/j.jmatprotec.2009.05.013

47. T. Durán, P. Pena, S. De Aza, J. Gómez-Millán, M. Alvarez, A.H. De Aza, Interactions in calcium aluminate cement (CAC)-based castables containing magnesia-Part II: Hydration-dehydration behavior of CAC and their mixtures with dead-burned and reactive-grade MgO, J. Am. Ceram. Soc. 94 (2011) 909–917. https://doi.org/10.1111/j.1551-2916.2010.04299.x

48. P.I.B.G.B. Pelissari, R.A. Angélico, V.R. Salvini, D.O. Vivaldini, V.C. Pandolfelli, Analysis and modeling of the pore size effect on the thermal conductivity of alumina foams for high temperature applications, Ceram. Int. 43 (2017) 13356-13363. https://doi.org/10.1016/j.ceramint.2017.07.035

49. P. Sepulveda, W.N. dos Santos, V.C. Pandolfelli, J.C. Bressiani, R. Taylor, Thermal conductivity of gelcast porous alumina, Am. Ceram. Soc. Bull. 78 (1999) 61–66.

50. D. Zacherl, M. Schnable, A. Buhr, G. Buchel, R. Kockegey-Lorenz, J. Dutton, Advantages of calcium hexaluminate in a corrosive environment, Refractories Worldforum 3 (4) (2011) 87-94.

51. R. Salomão, C.C. Arruda, V.C. Pandolfelli, L. Fernandes, Designing high-temperature thermal insulators based on densification-resistant in situ porous spinel (*In press, Corrected Proof*), J. Eur. Cer. Soc. (2021). https://doi.org/10.1016/j.jeurceramsoc.2020.12.014

Annex A: Preliminary evaluation of raw materials, calcium aluminate cement (CAC) content, and green dried samples

A.1. Introduction: Calcium aluminate cement as a hydraulic binder to ceramic suspensions

Calcium aluminate cement (CAC) is the most used hydraulic binder for high-alumina refractory castables systems [30,31]. It is added to compositions during mixing and connects particles through chemical reactions with water, restraining their movement after casting. The CAC's setting mechanism begins with the dissolution of calcium aluminates in water as Ca^{2+} and $(Al(OH)_4)^-$ ions up to the saturation of the medium [31,32]. Such a multi-ion solution remains stable for a certain time. After the formation of small solid nuclei at the surfaces of the surrounding particles, the precipitation of hydroxylated compounds begins to accelerate [38-40,44]. These sub-micron crystals exhibit a plate-like shape, hinder the movement of the surrounding matrix's particles, and reduce the volume of pores amongst them [43,44].

Such mechanisms increase both strength and rigidity of the structure and are temperature-time-dependent [38,39]. Reactions below 10 ℃ yield CAH_{10} as a hydrating product and require at least 5 days to fully harden the structure. On the other hand, those conducted above 10 ℃ result in C_2AH_8 (10-30 ℃) and C_3AH_6 (above 30 ℃) and show a faster and higher gain of strength [40,44]. After the curing period, the solid monolithic parts generated are strong and rigid enough to be demolded with no deformation. CAC's binding action also prevents drying shrinkage [30,31,39] and explosive spalling [35,36] caused, respectively, by capillarity forces and vapor pressurization during water withdrawal.

This section reports the preliminary tests aimed at determining a) the optimum curing conditions for maximizing the gain of strength and the amount of porogenic hydroxylated phases formed, and b) the range of CAC load added to the compositions that ensures minimal strength for handling, prevents excessive drying shrinkage, and avoids the formation of low-refractoriness compounds.

A.2 Materials and methods

Particles of the raw materials tested (calcium aluminate cement, CAC, EL70, Elfusa Geral de Eletrofusão, Brazil, and calcined alumina, CAl, E-sy 1000, Almatis, USA) were

previously characterized regarding morphology (field-emission-gun scanning electron microscopy, Inspect-F50, FEI, Netherlands), composition (X-ray dispersive spectroscopy, EDX 720, Shimadzu, Japan, after calcination at 1000 °C for 5 h), average and maximum particle diameter (D_{50} and D_{90}, respectively, DT-1202, Dispersion Technology Inc., USA), solid density (He pycnometry, Ultrapyc 1200e, Quantachrome Instruments, USA), specific surface area (BET N_2 adsorption, Nova 1200e, Quantachrome Instruments, USA, ASTM C 1069-09 standard), and loss of ignition (thermogravimetry, TGA-Q50, TA Instruments, 25-1000 °C, 5 °C.min^{-1} heating rate, synthetic air atmosphere).

The compositions were prepared initially dry-blending different proportions of CAC and CAl (Table 1) with a poly(ethylene glycol)-based dispersant (0.2 wt%, dry-basis, FS20, BASF, Germany). They were mixed with distilled water by a paddle mixer (PowerVisc, IKA, Germany, 1000 rpm, 5 min) towards forming suspensions containing 50 vol% of solids, which were cast as cylinders of 70 mm length × 16 mm diameter for the preliminary tests. Curing trials at 60 °C for 1 to 168 h in a moisture saturated atmosphere provided the time of completion of the curing process and the crystalline phases formed [35,38,39]. After regular intervals, 5 samples were demolded, dried at 120 °C for 24 h, and tested for flexural Young's modulus, flexural strength, total porosity, and drying shrinkage, as described in what follows. Each result is their average value (standard deviation represented by error bars).

Flexural Young's modulus (E, GPa) was measured at room temperature (25°C) by Impulse Excitation of Vibration Technique (Grindosonic HT, Belgium), according to ASTM E 1876-01 standard ("Standard Test Method for Dynamic Young's Modulus, Shear Modulus, and Poisson's Ratio by Impulse Excitation of Vibration"). The samples' flexural strength was measured at room temperature (25 °C) by three-point bending tests (MTS 810 TestStar II tensile tester; 2 N.s^{-1} loading rate; ASTM C78: "Standard Test Method for Flexural Strength of Concrete Using Simple Beam with Third-Point Loading"). Their total porosity was calculated with the use of their geometry (diameter and length) and mass, and solid density was measured by Helium pycnometry (after crushing, particle size below 100 µm) [3,4,6,14].

The length of hardened samples was measured before (L_{Green}) and after drying at 120 °C (L_{Dried}), and their linear dimensional change (LDV, %) was calculated concerning the corresponding initial length (negative values represent shrinkage, and vice-versa).

Both samples' morphology and crystalline phases were studied, respectively, in fracture surfaces by scanning electron microscopy, and X-ray diffraction (Rotaflex RV 200B, Rigaku-Denki Corp., Japan, Cu Kα radiation, λ = 0.14506 nm, in the 2θ range from 15 to 75° at 0.5

°.min^{-1} scan rate) combined with Rietveld refinement (MATCH! software, 3.8 version, Germany) [42].

A.3. Results and discussion

Table 1 and Figs. A.1a-c, respectively, display the physical properties and morphology of the as-received anhydrous CAC and CAl particles. Despite the differences expected in chemical composition and density, they show similar geometry and average size. The particles resulting from CAC's hydroxylation, on the other hand, are significantly smaller and precipitate in the spaces amongst CAl particles and on their surfaces (Fig. A.1d-f). Consequently, the higher the CAC content, the less porous the structure. Although such features related to the CAC hydration process have been described elsewhere [28,30,39,40,43,44], they are important for the understanding of the evolution of the samples' microstructure and pores formation during the initial heating.

Table 1

Figure A.1

Towards the production of structures comprised of stoichiometric calcium hexaluminate or calcium hexaluminate and alumina, the proportions of CAC and CAl were based on their full conversion into CA_6 [5,6,12]. For the particular grade used (Table 1), the maximum CAC content for a full conversion into stoichiometric CA_6 was 34 vol.%.

Fig. A.2 displays the combined effect of varying CAC load and curing time at 60 °C on the samples' rigidity, flexural strength, total porosity, and drying shrinkage. Typically, curing processes conducted between 10 and 30 °C result in different hydroxylated compounds (e.g., C_2AH_8, C_3AH_6, and $Al(OH)_3$ [37-39]). However, at such low curing temperatures, the gain in strength is slow, and up to seven days might be necessary for the reaching of the strength's maximum value [39]. On the other hand, during the curing trials conducted at 60 °C for 1 to 168 h, no significant change occurred in the samples' rigidity after the initial 24 h (Fig. A2.a). According to Figure A.3, for the samples with the highest CAC content (34 vol.% CAC) cured at 60 °C for 24 h, the crystalline phases formed a mixture of α-Al_2O_3 (from calcined alumina), C_3AH_6, and $Al(OH)_3$, and no peaks of anhydrous CAC phases were detected by XRD. Therefore, curing was considered complete after 24 h, and the standard curing

conditions for all compositions were set at 24 h at 60 °C under a moisture saturated atmosphere.

The original CAC content in the formulations affected their dried rigidity, strength, total porosity, and shrinkage (Fig. A.2b-c). As the CAC content increased (*i.e.* higher volume of CAC hydrates), progressive gains of rigidity, flexural strength, and dimensional stability were observed, whereas total porosity decreased. Regarding the minimum CAC load required for the production of stable structures, samples containing less than 10 vol.% of CAC showed a drying shrinkage above 0.5 %, which is the generally assumed safety limit [30,31], therefore, they were no longer tested.

Figure A.2

Figure A.3

A.4 Conclusions

The curing conditions for maximizing CAC bonding action and hydrated compounds formed were 24 h at 60 ºC, in a high-humidity environment. Minimum CAC load to ensure dimensional stability after drying: 10 vol.%. Maximum CAC load to form stoichiometric CA_6, preventing the generation of lower melting point aluminates: 34 vol. %.

Annex B: Complete XRD patterns for samples containing 34 vol.% of CAC heat-treated at different temperatures (120-1500 °C) for 3 h. Figure 2 shows a compilation of the results.

Figure B.1

Figures captions

Figure 1: Thermogravimetric analysis of green humid samples (freshly demolded) containing different CAC contents: a) Mass loss and temperature *versus* time curves; mass loss rate and temperature *versus* time curves during b) removal of free water, and c) removal of combined water from hydrated phases.

Figure 2: Relative weight fraction of crystalline phases for samples containing 34 vol.% of CAC heat-treated at different temperatures (120-1500 °C) for 3 h.

Figure 3: SEM images of the fracture surface of samples containing 34 vol.% of CAC after heat treatment for 3 h at: a) 120 °C; b) 300 °C; c) 500 °C; d) 700 °C; e) 900 °C; f) 1100 °C; g) 1300 °C; and h) 1500 °C.

Figure 4: Samples containing 10 vol.% of CAC: a) Effect of heat treatment temperature on flexural Young's modulus, flexural strength, and total porosity; and b) Dilatometric analysis.

Figure 5: Samples containing 20 vol.% of CAC: a) Effect of heat treatment temperature on flexural Young's modulus, flexural strength, and total porosity; and b) Dilatometric analysis.

Figure 6: Samples containing 34 vol.% of CAC: a) Effect of heat treatment temperature on flexural Young's modulus, flexural strength, and total porosity; and b) Dilatometric analysis.

Figure 7: XRD patterns for samples containing different amounts of CAC and heat treated at 1500 °C for 3 h. Symbols identification (JCPDS file): O = α-Al_2O_3 (46-1212); ✱ = CA_6 or $CaAl_{12}O_{19}$ (38-470).

Figure 8: SEM images of the fracture surface and pore size distribution of samples prepared with different CaO sources: 34 vol.% CAC (present work) and 19 vol.% $CaCO_3$ (D_{50} = 15 μm, from the literature [14]) after heat treatment at 1500 °C for 3 h. APS = Average pore size, TP = Total porosity, E = Flexural Young's modulus, FS = Flexural strength.

Figure 9: Dependence of thermal conductivity on temperature for the sample containing 34 vol.% of CAC previously sintered at 1500ºC for 3 h. References' results are also shown [14,50-52].

Figure A.1: SEM images of the morphology of as-received particles of a-b) calcium aluminate cement (CAC), and c) calcined alumina (CAl), and of the fracture surface of dried samples (120 °C, 24 h) containing d) 10 vol.%, e) 20 vol.%, and f) 34 vol.% of CAC.

Figure A.2: Effect of curing time at 60 °C on a) flexural Young's modulus of dried samples containing different amounts of calcium aluminate cement (CAC). Effect of varying CAC content on the properties of dried samples (cured at 60 °C for 24 h): b) flexural Young's modulus and drying linear change, and c) total porosity and flexural strength.

Figure A.3: XRD pattern for samples containing 34 vol.% of CAC dried at 120 °C for 24 h. Symbols identification (JCPDS file): O = α-Al_2O_3 (46-1212); ● = C_3AH_6 or $Ca_3Al_2(OH)_{12}$ (2-1124); ◇ = α-$Al(OH)_3$ (29-41).
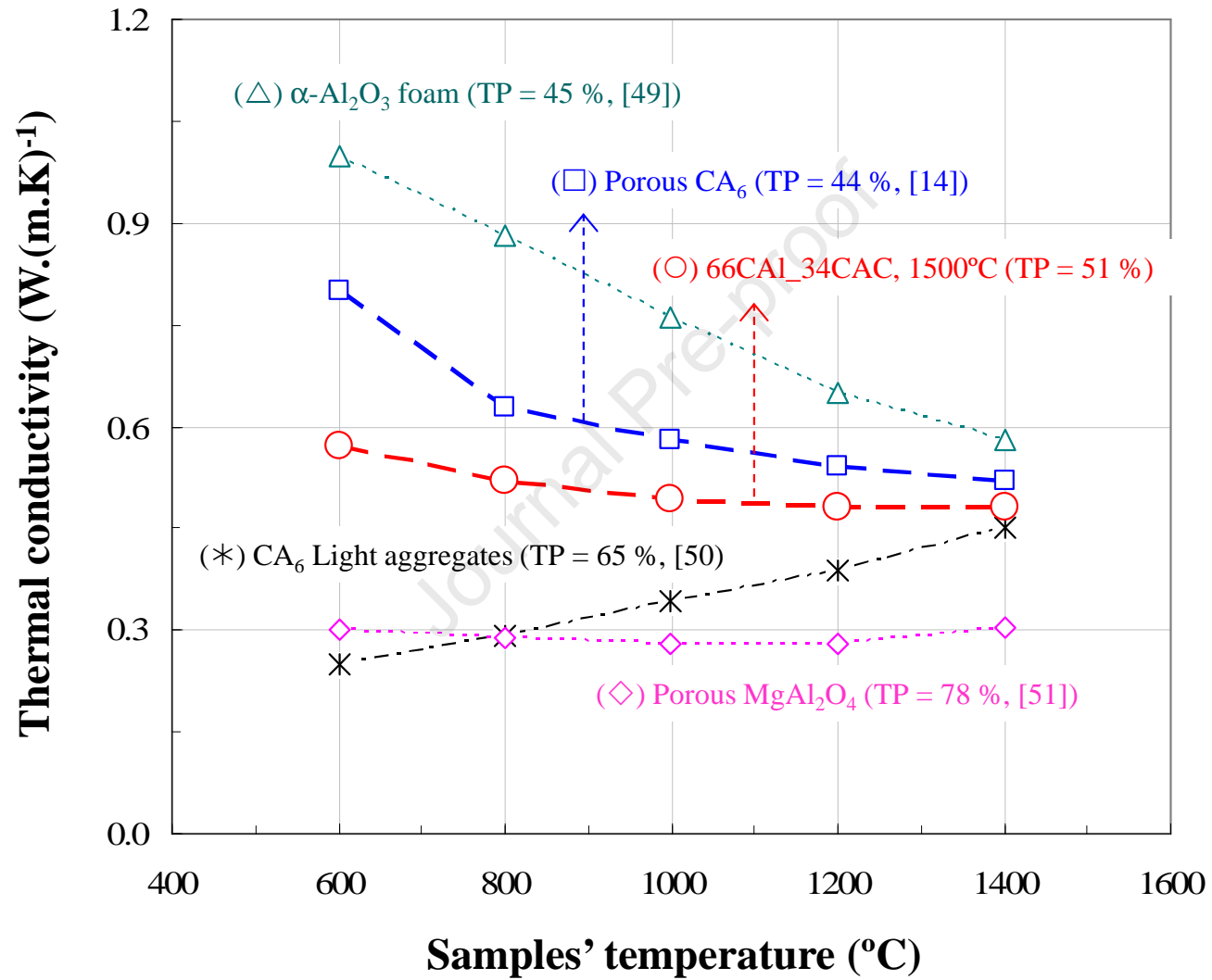
Figure B.1: XRD patterns for samples containing 34 vol.% of CAC heat treated at different temperatures (120-1500 °C) for 3 h. Symbols identification (JCPDS file): $\bigcirc$ = α-Al_2O_3 (46-1212); $\bullet$ = C_3AH_6 or $Ca_3Al_2(OH)_{12}$ (2-1124); $\diamondsuit$ = α-$Al(OH)_3$ (29-41); $\blacktriangle$ = C_3A or $Ca_3Al_2O_6$ (32-150); $\square$ = $C_{12}A_7$ or $Ca_{12}Al_{14}O_{33}$ (48-1882); $\triangledown$ = CA_2 or $CaAl_4O_7$ (72-767) ; $\ast$ = CA_6 or $CaAl_{12}O_{19}$ (38-470).

Table 1: Raw materials and compositions tested.

Physical properties		Calcined alumina (CAl)	Calcium aluminate cement (CAC)
Composition (wt.%)	Al_2O_3	99.4	67.4
	Na_2O	0.20	0.13
	Fe_2O_3	0.03	0.43
	SiO_2	0.34	3.60
	CaO	0.03	28.1
	MgO	-	0.34
Particle size (μm)		D_{50} = 1.5 / D_{90} = 9.6	D_{50} = 2.0 / D_{90} = 6.0
Solid density (g.cm^{-3})		3.97	3.23
Specific surface area (m^2.g^{-1})		1.3	0.6
Loss of ignition (wt. %, 5h, 1000 °C)		< 0.1	< 0.1

| Compositions identification | Al_2O_3/CaO molar fractions | Composition before firing (vol.% / wt.%) | | Fraction of phases formed at 1500°C | | | |
				Theoretical (wt.%, [5,6,14])		Experimental (wt.%, Fig. 7)	
		CAl	CAC	α-Al_2O_3	CA_6	α-Al_2O_3	CA_6
[a] 100CAl_0CAC	1.00/0.00	100/100	0.0/ 0.0	100	0.0	-	-
[a] 98CAl_02CAC	0.99/0.01	97.5/97.9	2.5/2.1	92.8	7.2	-	-
[a] 95CAl_05CAC	0.98/0.02	95/95.9	5.0/4.1	85.8	14.2	-	-
90CAl_10CAC	0.96/0.04	90/91.7	10/8.3	71.6	28.4	74.1	25.9
80CAl_20CAC	0.92/0.08	80/83.1	20/16.9	42.3	57.7	45.6	54.4
[b] 66CAl_34CAC	0.86/0.14	66/70.7	34/29.3	0.0	100	10.2	92.7

a) Compositions considered unsuitable for casting during the preliminary tests (Annex A); b) Composition to form stoichiometric CA_6
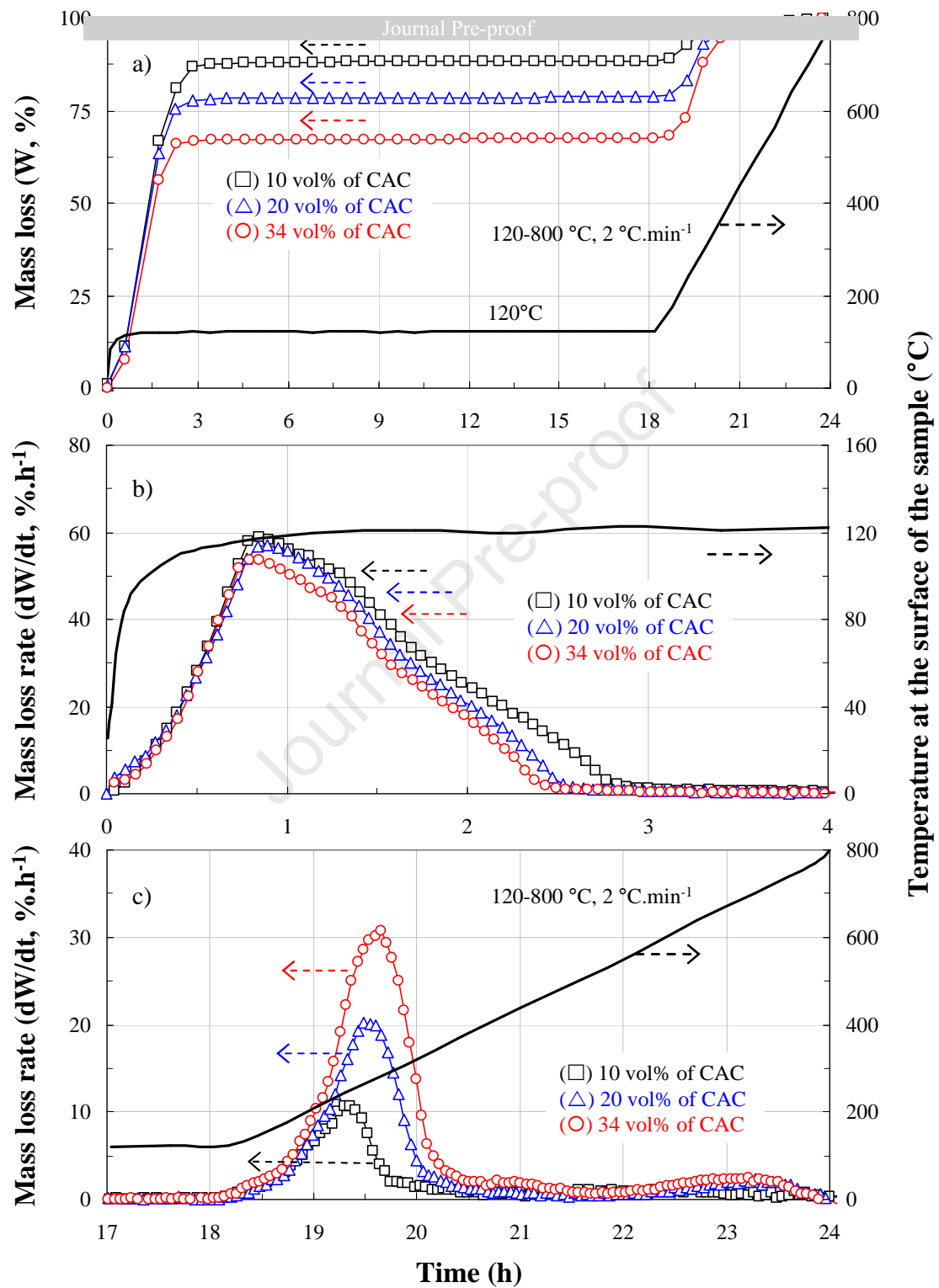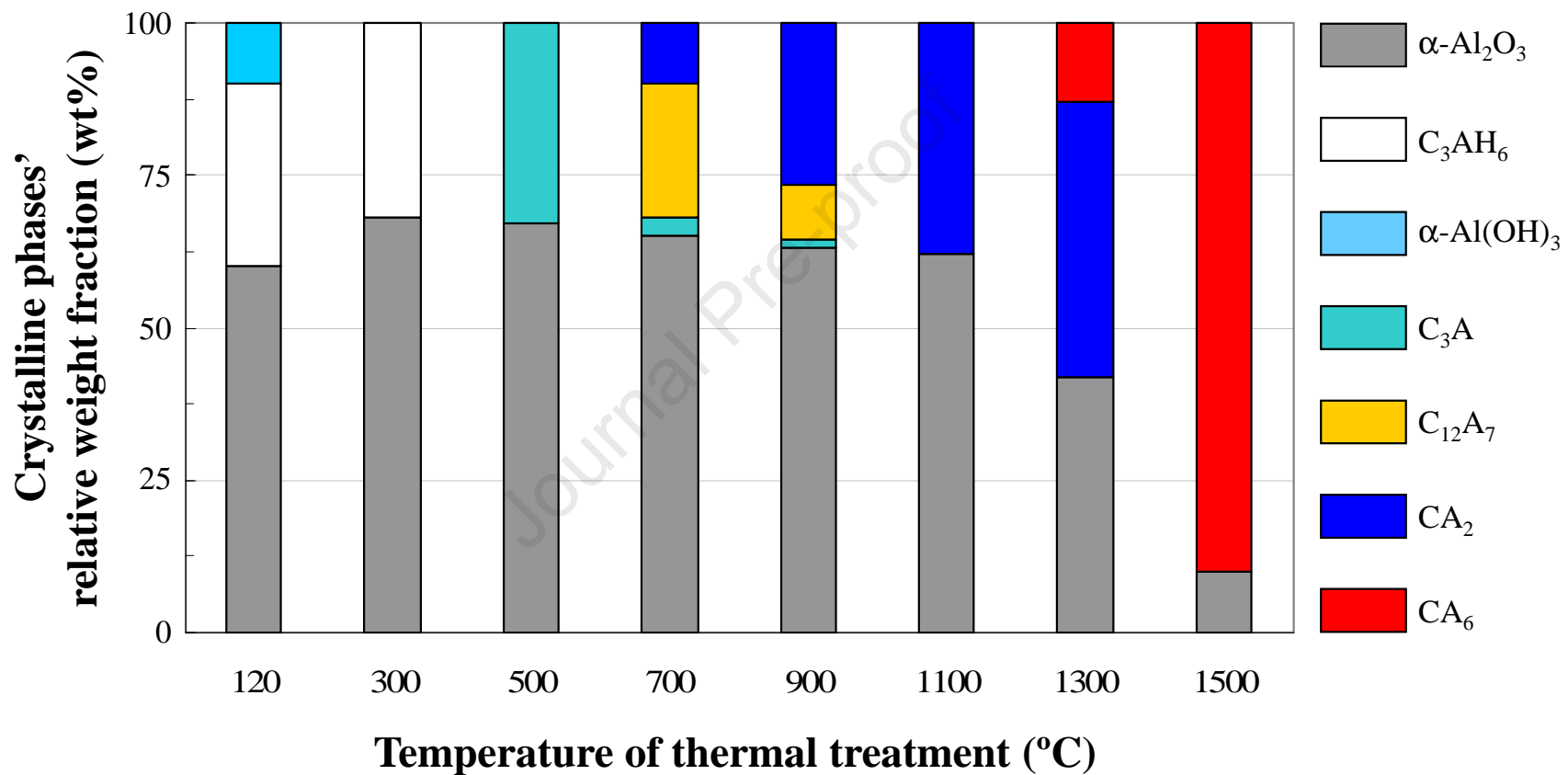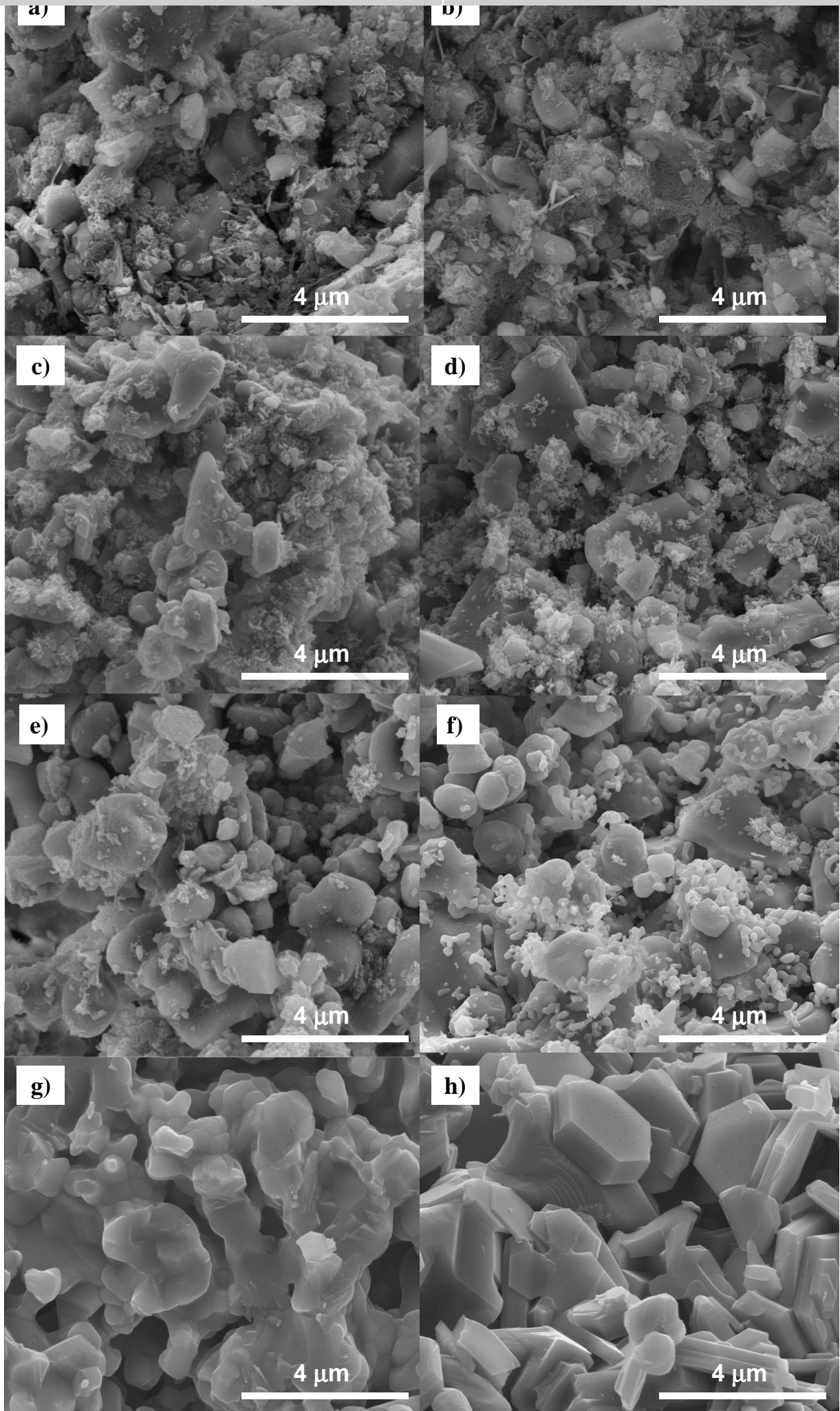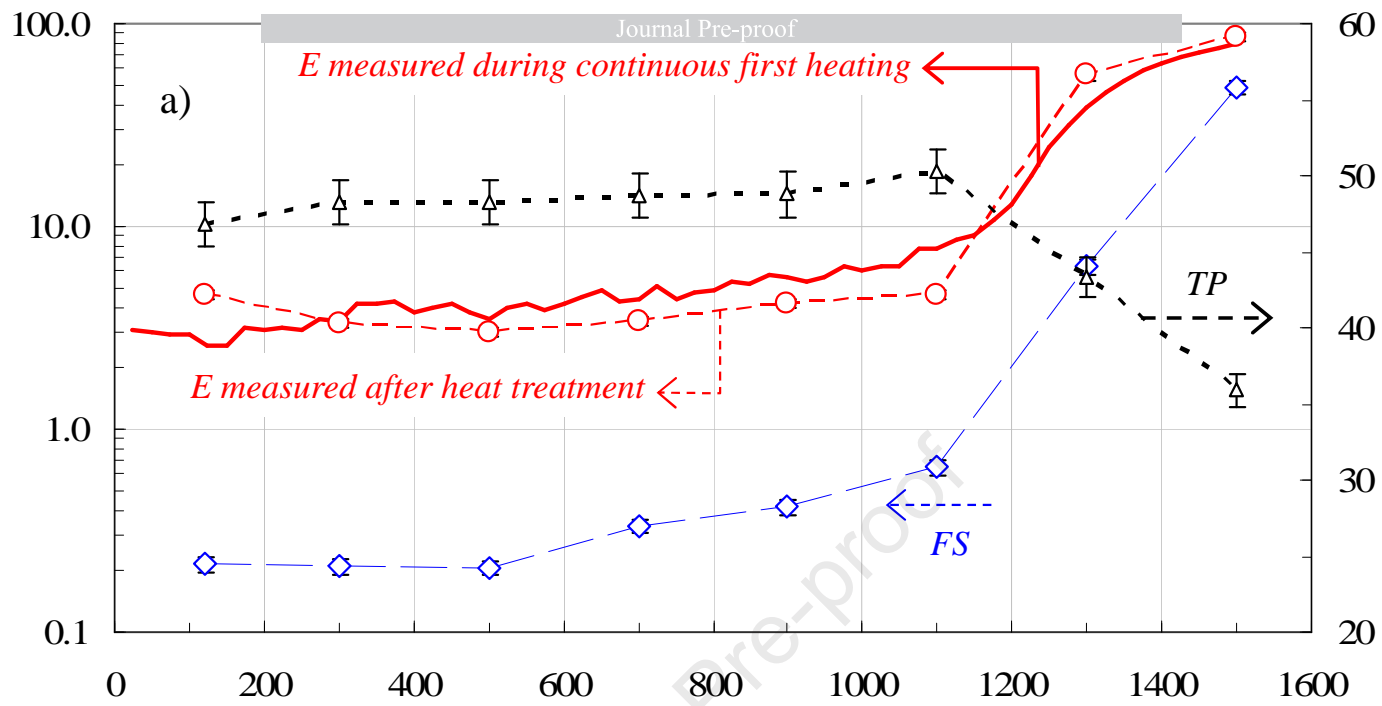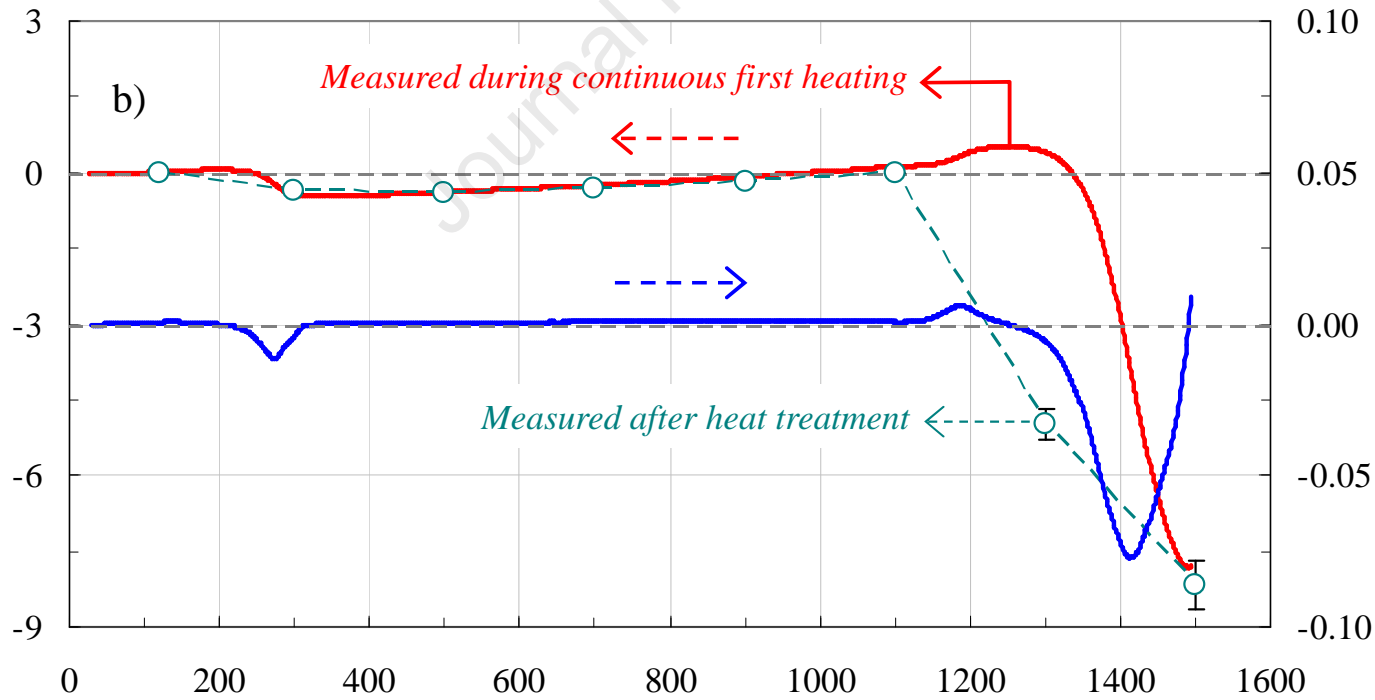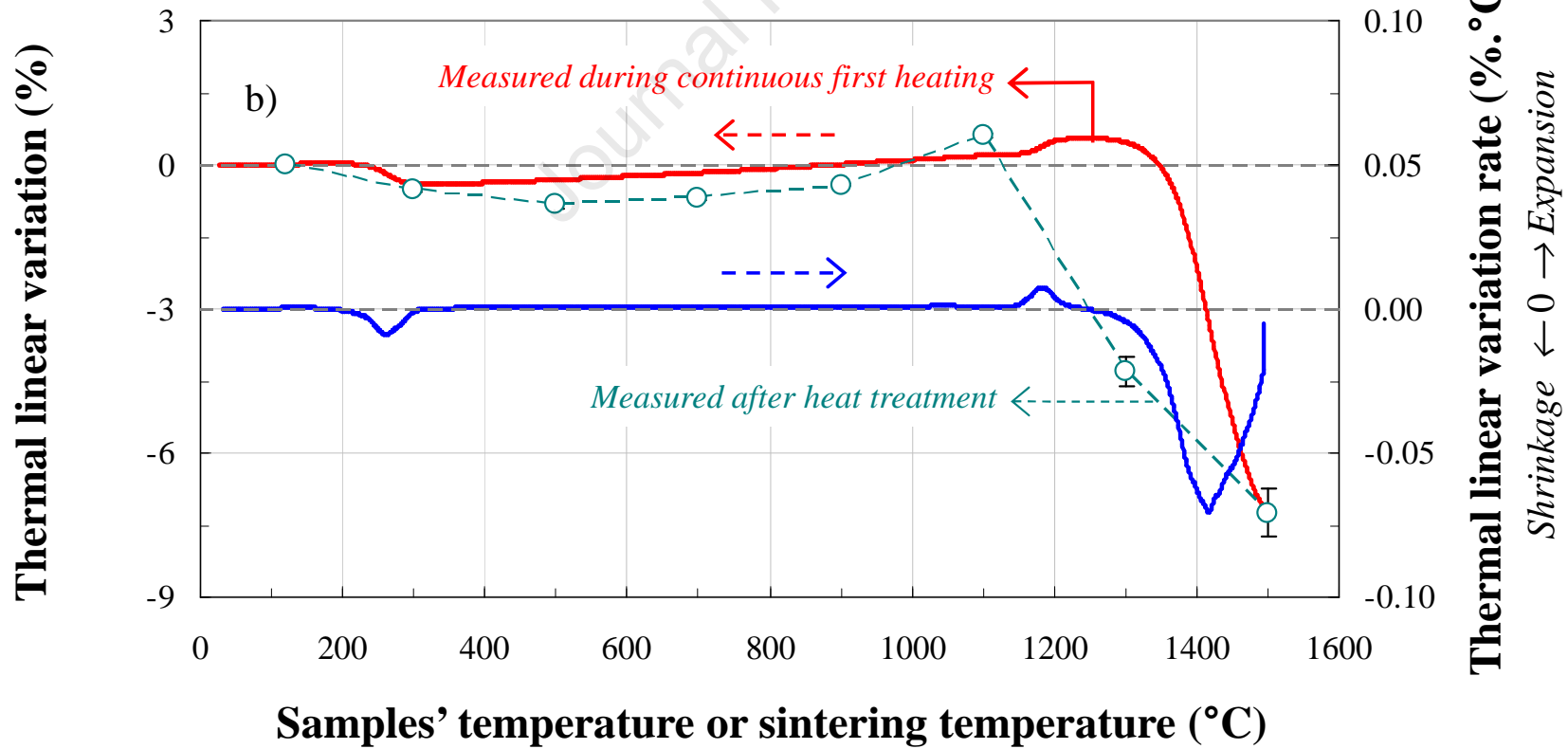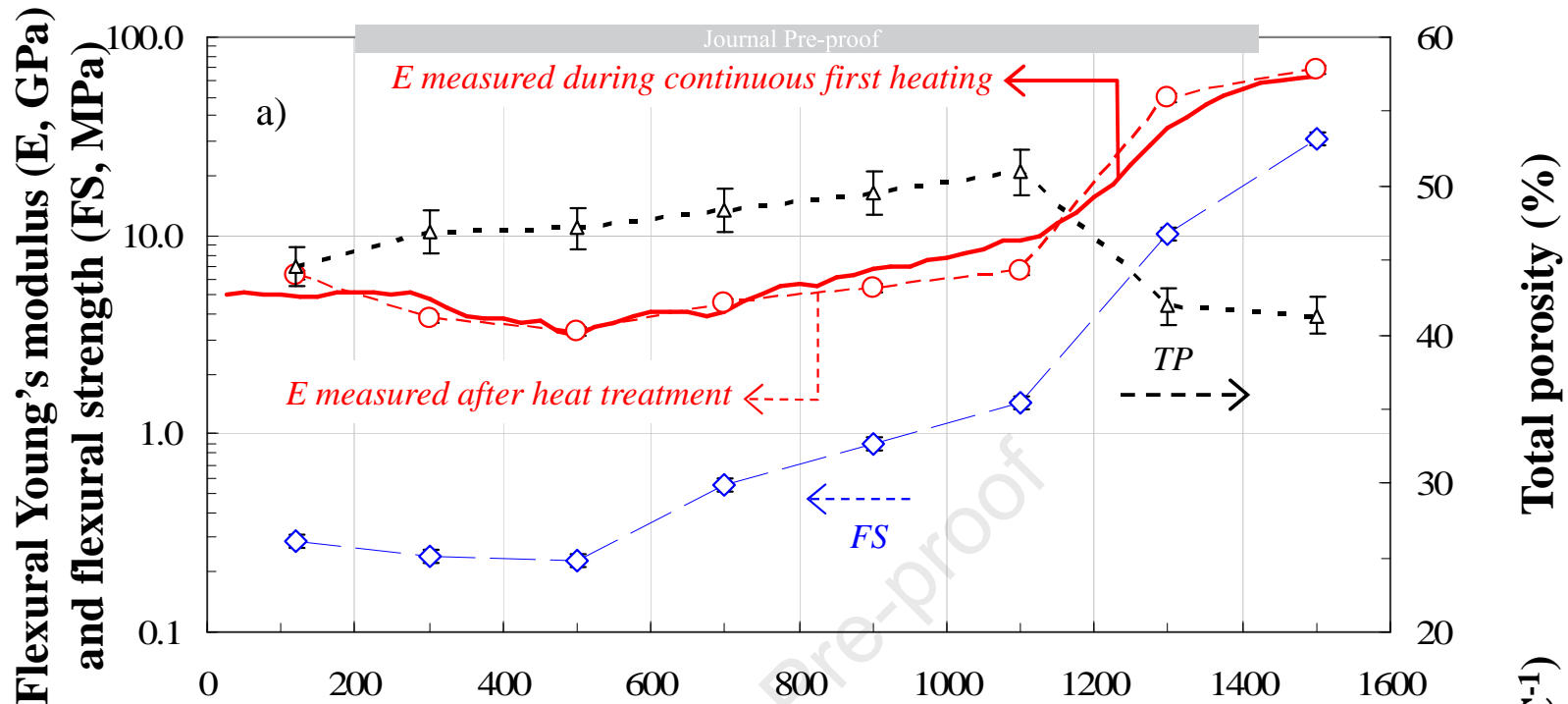
$(\triangle)$ α-Al_2O_3 foam (TP = 45 %, [49])

$(\square)$ Porous CA_6 (TP = 44 %, [14])

$(\bigcirc)$ 66CAl_34CAC, 1500ºC (TP = 51 %)

$(\ast)$ CA_6 Light aggregates (TP = 65 %, [50])

$(\diamondsuit)$ Porous $MgAl_2O_4$ (TP = 78 %, [51])

34 vol.% CAC, 1500 °C
D_{50} C_3AH_6: 80-200 nm
$APS_{1500°C}$: 0.5 µm
TP: 51 %
E = 51 GPa
FS = 21 MPa

Reference [14]
D_{50} $CaCO_3$: 15 µm
$APS_{1500°C}$: 16 µm
TP = 44 %
E = 88 GPa
FS = 40 MPa
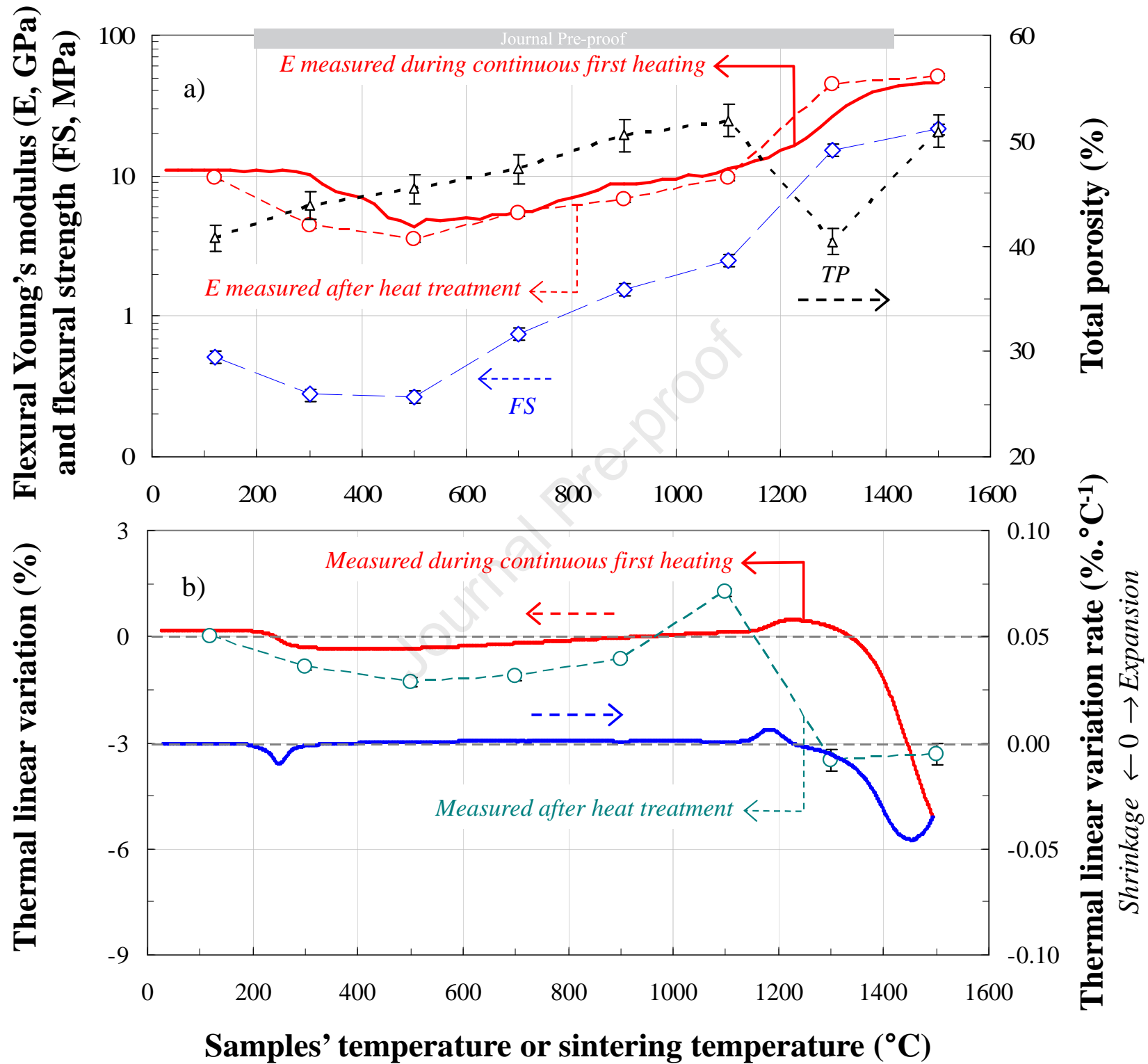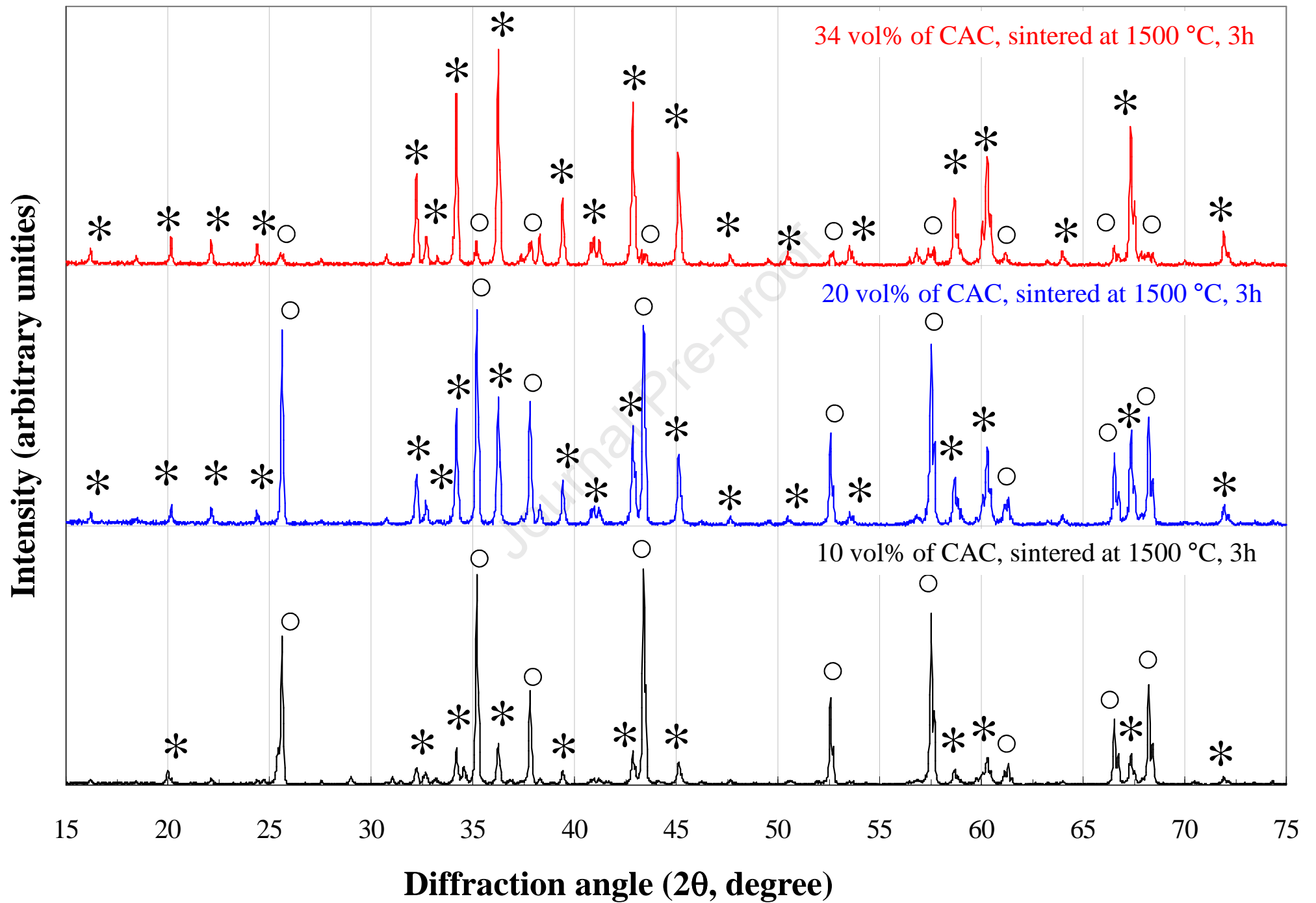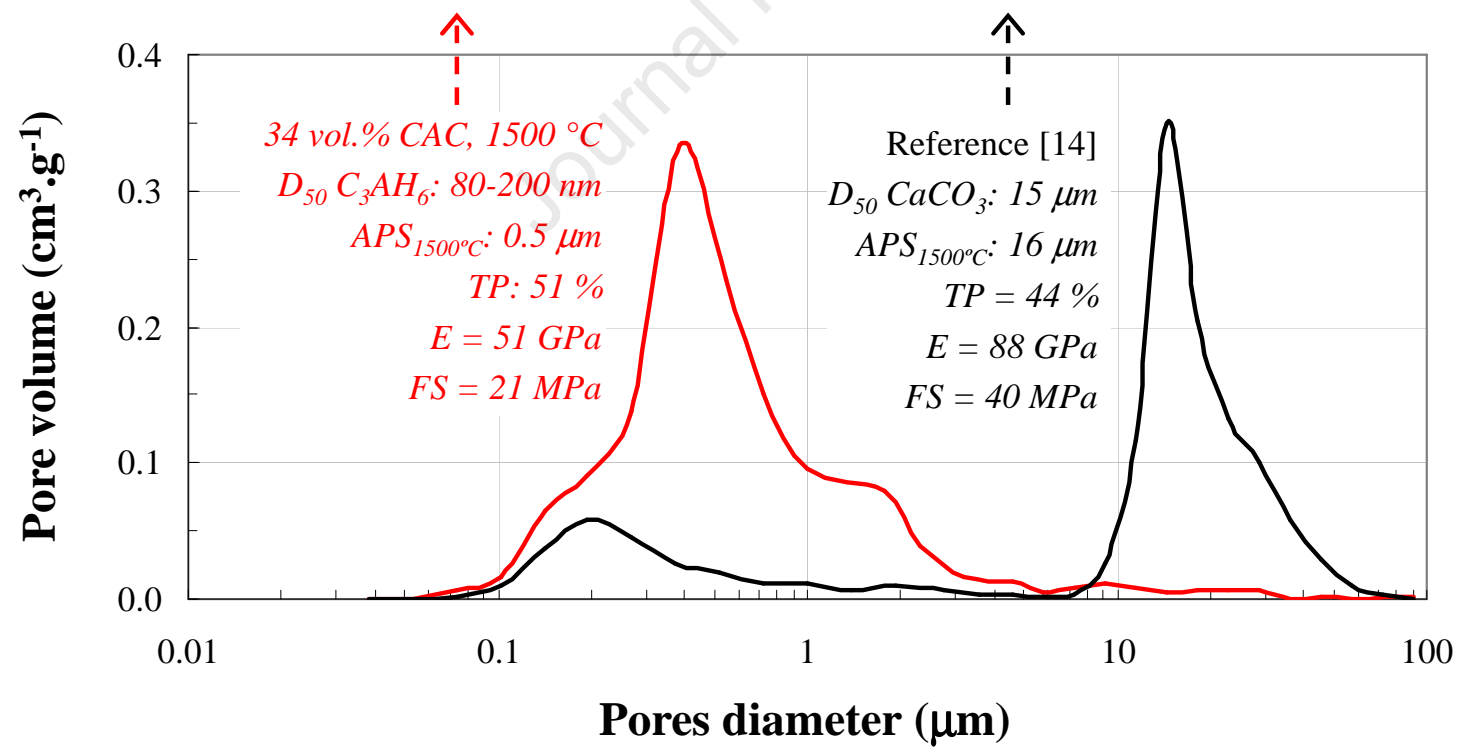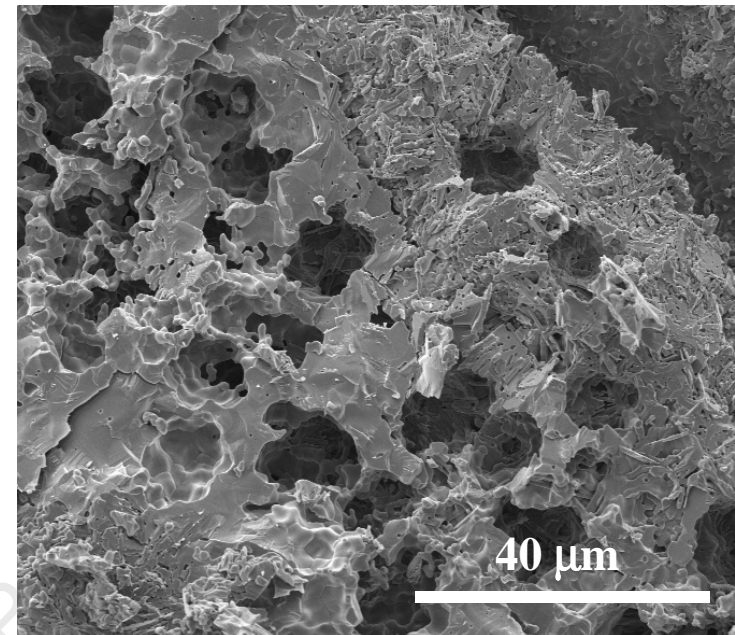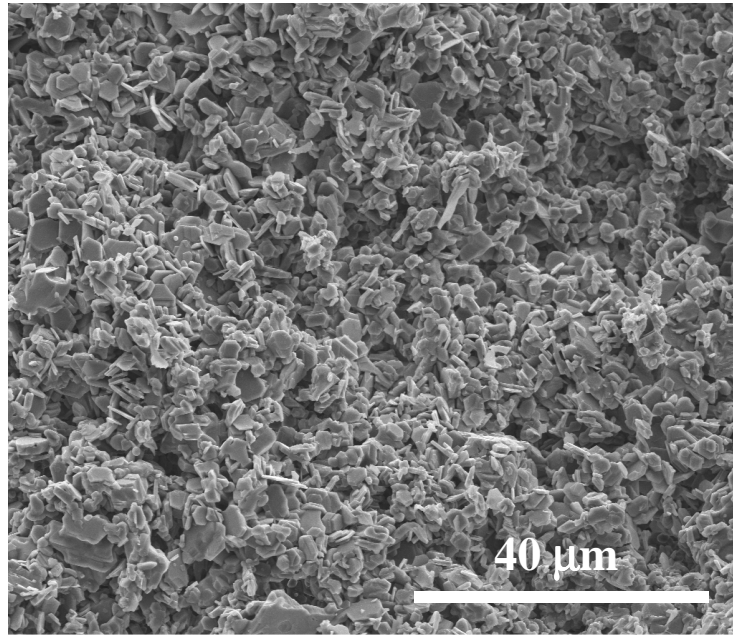
Declaration of interests

☒ The authors declare that they have no known competing financial interests or personal relationships that could have appeared to influence the work reported in this paper.

☐The authors declare the following financial interests/personal relationships which may be considered as potential competing interests: